Longitudinal analysis of diffusion-weighted MRI with a ball-and-sticks model

Arkesteijn, G. A.M.; Poot, D. H.J.; Niestijl, M.; Vernooij, Meike W.; Niessen, W. J.; Van Vliet, L. J.; Vos, F. M.

DOI
10.1109/ISBI.2017.7950635

Publication date
2017

Document Version
Accepted author manuscript

Published in
2017 IEEE 14th International Symposium on Biomedical Imaging, ISBI 2017

LONGITUDINAL ANALYSIS OF DIFFUSION-WEIGHTED MRI WITH A BALL-AND-STICKS MODEL

G.A.M. Arkesteijn[1,2,3], D.H.J. Poot[1,2,3], M. Niestijl[1], M.W. Vernooij[3,4], W.J. Niessen[1,2,3], L.J. van Vliet[1], F.M. Vos[1,5]

[1] Quantitative Imaging Group, Delft University of Technology, Delft, the Netherlands
Depts. of: [2] Medical Informatics, [3] Radiology, [4] Epidemiology, Erasmus MC, Rotterdam, the Netherlands
[5] Dept. of Radiology, Academic Medical Center, University of Amsterdam, the Netherlands

ABSTRACT

Purpose: To increase the sensitivity in longitudinal analysis of DW-MRI data with the ball-and-sticks model.
Methods: Longitudinal DW-MRI data (baseline and two follow-up scans) of 25 middle-aged subjects (47 to 61 years at base line) were acquired. After coregistering all the diffusion-weighted images (DWIs) from the baseline and follow-up scans to a subject-specific intermediate space, an extended ball-and-sticks model was fitted. Stick orientations were constrained such that they did not change over time. The stick fractions were warped and projected onto the TBSS (tract-based spatial statistics) skeleton, and were compared to a reference framework in which all scans were processed independently.
Results: Compared to the reference framework, the standard deviation of the apparent noise on the primary stick fractions on the TBSS skeleton was reduced with approximately a factor two.
Conclusion: The use of the proposed longitudinal DW-MRI pipeline may significantly increase the precision compared to a default cross-sectional image processing pipeline.

***Index Terms*—** DW-MRI, longitudinal, ball-and-sticks

1. INTRODUCTION

Diffusion-weighted magnetic resonance imaging (DW-MRI) is a non-invasive MRI technique that enables measurement of diffusion of water [1]. It is frequently used to assess the brain's white matter integrity, because the water diffusivity reflects the microstructural organization of neural fibers [2].

The quantitative nature of DW-MRI makes it especially suitable for longitudinal studies because it facilitates measurement of subject-specific changes in diffusion behavior. Longitudinal studies in DW-MRI have for instance been used to quantify small changes in the white matter after ischemic stroke [3], during development [4], and during normal ageing [5].

A limitation of many DW-MRI studies (e.g. [3-5]) is in the use of the conventional single tensor model. It is well known that water diffusion in white matter cannot be adequately modeled by a Gaussian, particularly in voxels containing more than one fiber tract. Therefore, diffusion descriptors computed from this model may lack sensitivity [6], or may suggest spurious change in the white matter microstructure [7, 8].

Several alternative models have been proposed to provide a more adequate description of the diffusion including the ball-and-sticks model [9], multi-tensor models [10], or CHARMED [11]. However, the number of unknown parameters is larger in these models, which hinders precise estimation.

Particularly in a longitudinal DW-MRI study it is of interest that a good precision is achieved, because the effect size is typically small. Simultaneously, however, a longitudinal study offers the opportunity to pool information across different scans of the same subject. For instance, in many DW-MRI studies it seems reasonable that the orientation of white matters does not change drastically over the time span of a few years. This would allow the estimated white matter orientations to be constrained over time. In effect this reduces the total number of unknown parameters, which could enhance the precision of parameter estimation.

The goal of our paper is to increase the sensitivity of longitudinal DW-MRI studies using the ball-and-sticks model. The key novelty of our approach is that we coregister the DWIs from the baseline and follow-up scans from the same subject and then fit a ball-and-sticks model to all DWIs simultaneously. While doing so the stick orientations are constraint to be the same on the different time points. All other unknown ball-and-sticks parameters are estimated separately for each time point. We evaluate the proposed method with diffusion data from 25 subjects.

2. MATERIALS & METHODS

2.1. Overview of proposed framework

In Figure 1 an overview of the proposed framework is presented. After basic preprocessing, the DWIs from the baseline and follow-up scans are coregistered to a subject-

specific intermediate space. Next, an extended ball-and-sticks model is fitted to all DWIs simultaneously. In this extended ball-and-sticks model, the stick orientations are constrained across the different scans. All other unknown parameters are still estimated for each scan. In the following sections, each of these steps will be discussed in more detail.

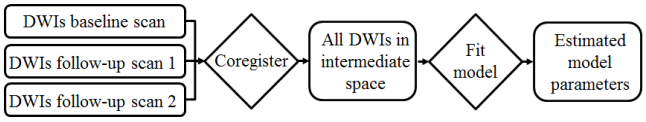

Figure 1. Overview of the proposed framework for fitting a diffusion model to the DWIs of a single subject.

2.2. Study population

The proposed framework was evaluated on 25 middle-aged subjects (47 to 61 years at base line) from the Rotterdam Study, a prospective population-based cohort study among middle-aged and elderly subjects in a district of the city of Rotterdam, the Netherlands [12]. Ethical approval was granted by the institutional review board, and written informed consent was obtained from all participants.

2.3. Data acquisition

All subjects were scanned three times on a 1.5 Tesla MRI scanner (GE Signa Excite) using an 8-channel head coil. The average time between baseline scan and last follow-up scan was 5.8 years. No major hardware or software updates were performed on the scanner throughout the study [13]. DWIs were acquired with a single shot, diffusion-weighted spin echo echo-planar imaging sequence using TR = 8575 ms, TE = 82.6 ms, FOV = 210x210 mm^2, imaging matrix = 96x64 (zero-padded to 256x256), yielding 35 contiguous slices with a thickness of 3.5 mm. DWIs were acquired in 25 non-collinear directions with a b-value of 1000 s/mm^2. Three volumes were acquired without diffusion-weighting (the b_0-volumes) [13].

2.4. Preprocessing

The DWIs from each baseline and follow-up scan were separately corrected for motion and eddy current distortion by affine coregistration to the b_0-volume using `flirt` (part of FSL [14]). After coregistration to the reference b_0-volume, the gradient directions were reoriented according to the rotation component of the transformation [15]. Then, a single tensor model was fitted separately fitted to the DWI baseline and follow up data merely to facilitate mutual coregistration.

2.5. Coregistration of DWIs

The DWIs from the baseline and both follow-up scans were transformed to a subject-specific intermediate space. While doing so, it is essential to avoid any asymmetry bias [16]. We therefore extended the approach in [5] to support three scans. An overview is presented in Figure 2.

Let A, B and C refer to the scans at three different time points. First, based on the FA (fractional anisotropy), all pairwise (nonrigid) transformations (i.e. T_{AB}, T_{BA}, T_{BC}, T_{CB}, T_{AC}, T_{CA}) were computed using `fnirt` (part of FSL). Next, the transformation to intermediate space M was computed by inverting and adding the displacement fields, e.g. $T_{AM} = \text{inv}(T_{BA})/3 + \text{inv}(T_{CA})/3$.

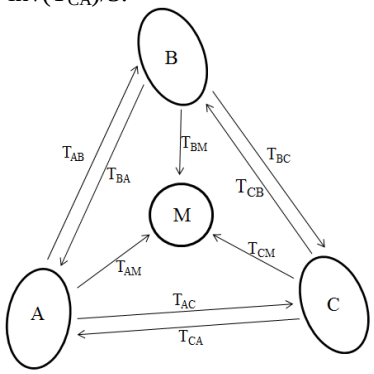

Figure 2. Overview of the coregistration of the DWIs from three different scans.

The affine transformations applied during preprocessing (motion end eddy current distortion correction) were concatenated with the nonrigid transformations to the subject-specific intermediate space, such that only a single interpolation of the DWIs was required. Simultaneously, the DWIs were upsampled to 2.0 mm^3 cubic resolution. After this transformation, the corresponding gradient directions were globally reoriented [15].

2.6. Reference ball-and-sticks model

In the ball-and-sticks model [9], the diffusion-weighted signal in the *i*-th DWI is modeled as follows:

$$S_{\boldsymbol{\theta},i} = S_0\left(\left(1-\sum_{j=1}^{N} f_j\right)exp(-b_i d) + \sum_{j=1}^{N} f_j exp\left(-b_i d\left(\mathbf{V}_j \cdot \mathbf{g}_i^T\right)^2\right)\right),$$

in which b is the diffusion-weighting parameter, $\mathbf{g}$ is a unit vector that specifies the direction of a diffusion-encoding gradient pulse, S_0 is the non-diffusion-weighted signal, N is the number of stick compartments, d is a diffusivity parameter, f_j represents a stick's volume fraction and $\boldsymbol{V}_j$ the principal eigenvector of the j-th stick compartment.

The function `bedpostx` (part of FSL [9]) was used to fit the ball-and-sticks model with N=2 stick compartments to each scan in its native space. After estimation, the stick fractions and orientations were warped to the subject-specific intermediate space, using the appropriate functions in FSL (i.e. `applywarp` and `vecreg`).

2.7. Longitudinal ball-and-sticks model

In the longitudinal ball-and-sticks model, the diffusion-weighted signal $\mathbf{S_0}$ in the i-th acquired DWI of the k-th scan is modeled according to:

$$S_{\boldsymbol{\theta},i,k} = S_{0,k}\left(\left(1-\sum_{j=1}^{N} f_{j,k}\right)exp\left(-b_{i,k}d_k\right) + \sum_{j=1}^{N} f_{j,k}exp\left(-b_{i,k}d_k\left(\mathbf{V}_j\cdot\mathbf{g}_{i,k}^T\right)^2\right)\right).$$

Here, the eigenvectors $\mathbf{V}_j$ are parameterized using spherical coordinates ψ_j and φ_j. In case of k=3 scans and N=2 stick compartments, the unknown parameter vector $\boldsymbol{\theta}$ becomes [$S_{0,1}$, $f_{1,1}$, $f_{2,1}$, d_1, $S_{0,2}$, $f_{1,2}$, $f_{2,2}$, d_2, $S_{0,3}$, $f_{1,3}$, $f_{2,3}$, d_3, ψ_1, φ_1, ψ_2, φ_2]. Notice that now the stick direction parameters (ψ_1, φ_1, ψ_2, φ_2) are the same for each scan k. A maximum likelihood estimator using a Rician noise distribution was used to estimate the unknown parameter vector in each voxel of the intermediate space [10].

2.8. TBSS analysis

The stick fractions of both the proposed (longitudinal) and reference framework were analyzed on a white matter skeleton in atlas space (FMRIB58) using TBSS (tract-based spatial statistics) [17]. The function `tbss_x` was used to warp and project the stick fractions onto a skeleton, which takes into account that partial volume fractions are not scalar measurements of diffusion but have orientations that need to be matched across subjects [18]. The ICBM-DTI-81 white matter label atlas [19] was warped to FMRIB58 space and used to label skeleton voxels, such that average stick fractions over different white matter structures could be computed.

3. EXPERIMENTS & RESULTS

In Figure 3 one example of stick orientations estimated with the reference framework are visualized. In single fiber regions, e.g. the corpus callosum (red circle), the sticks are similarly oriented in the three different scans. In crossing-fiber regions, however, the sticks have inconsistent orientations across the three scans (blue circle).

The between-scan differences of the primary stick fractions of the same subject are primarily caused by 'noise'. Therefore we take these between-scan differences as a measure of estimation variation. For each subject the standard deviation of the primary stick fractions f_1 across the three scans is computed in the TBSS skeleton voxels. In Figure 4 we show this standard deviation, averaged over the 25 subjects in our study. Observe that the average standard deviation of the proposed framework is only half that of the reference framework.

In Figure 5 the average within-subject standard deviation of the mean primary stick fractions in each of the 48 white matter structures in the ICBM-DTI-81 atlas is visualized. Again it can be observed that the proposed framework yields smaller between-scan differences. Finally, as an example, we visualize the average primary stick fractions obtained with the proposed framework in the 'Superior corona radiata R (label 25)' in Figure 6.

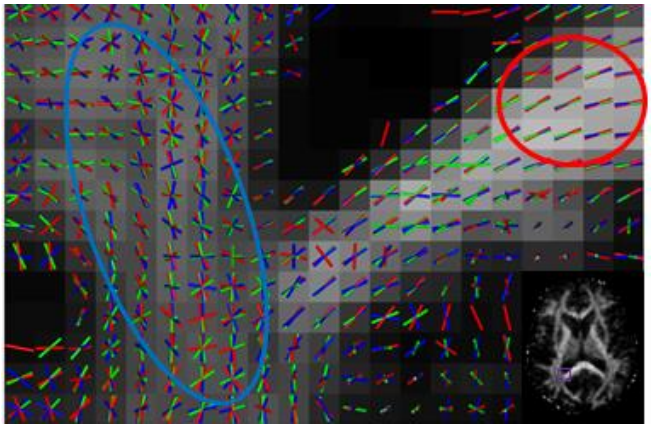

Figure 3. Example of stick orientations estimated from the baseline (red), the first follow-up (blue) and the second follow-up (green) scan of the same subject.

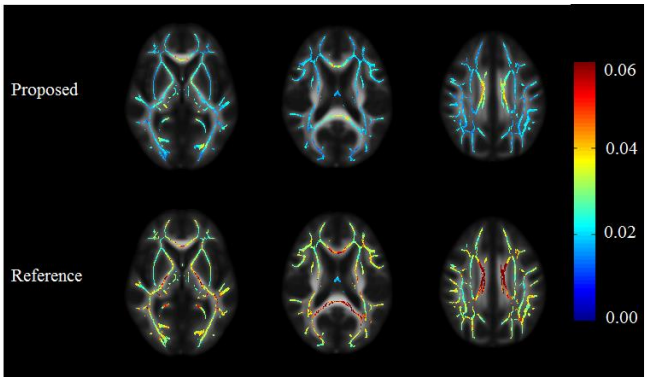

Figure 4. The average within-subject standard deviation of the primary stick fraction on a white matter skeleton.

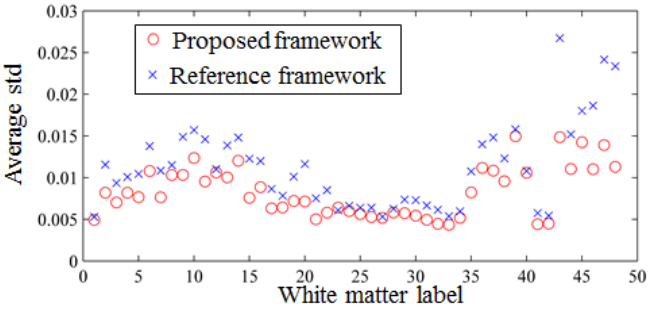

Figure 5. Average within-subject standard deviation of the primary stick fractions in 48 white matter structures.

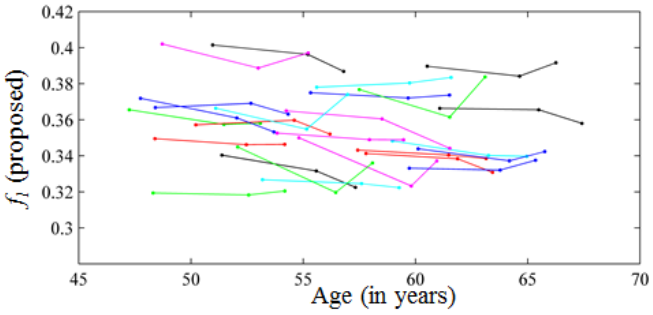

Figure 6. Example of primary stick fractions obtained with the proposed framework in the 'Superior corona radiata R (label 25)' versus age. Connected points represent the same subject. Lines have random colors to distinguish between different subjects.

4. DISCUSSION & CONCLUSION

We have evaluated a framework to simultaneously fit the ball-and-sticks model to multiple scans of the same subject. This approach allowed the stick-orientation to be constrained over different scans, while all other parameters were estimated separately for each scan.

We have limited our evaluation of the longitudinal framework to the ball-and-sticks model. More complex models of diffusion (e.g. [10] or [11]) were not supported by our DW-MRI data as they require the DWIs to be acquired with more than one non-zero *b*-value.

A non-rigid transformation was used to warp the scans to a subject-specific intermediate space. We preferred this approach over an affine or rigid transformation such that shrinkage of the brain and growth of the ventricles could be represented.

The advantage of constraining the orientations across different scans can be appreciated in Figure 3. The shown variation of the estimated stick orientations across scans simultaneously results in additional variance in the estimated stick fractions (see Figure 4 and Figure 5). Large fluctuations of the stick orientations across different scans may also affect the (orientation-based) labeling of the stick fractions used in `tbss_x` which will add to the variance on the skeletonized stick fractions. These are the primary reasons why the within-subject standard deviations of the stick fractions were much lower with the proposed framework.

The small within-subject fluctuations of the stick fractions suggest that the proposed framework may be more sensitive to subtle changes in the white matter, and may therefore be a promising tool in future longitudinal DW-MRI studies.

5. ACKNOWLEDGMENTS

This study was financially supported as part of the STW Perspectief programme Population Imaging Genetics (ImaGene) supported by the Dutch Technology Foundation (STW), project 12722.

6. REFERENCES

[1] Stejskal, E. and J. Tanner, *Spin diffusion measurements: spin echoes in the presence of a time-dependent field gradient.* The journal of chemical physics, 1965. **42**(1): p. 288-292.
[2] Beaulieu, C., *The basis of anisotropic water diffusion in the nervous system–a technical review.* NMR in Biomedicine, 2002. **15**(7-8): p. 435-455.
[3] Wang, C., et al., *Longitudinal changes in white matter following ischemic stroke: A three-year follow-up study.* Neurobiology of Aging, 2006. **27**(12): p. 1827-1833.
[4] Simmonds, D.J., et al., *Developmental stages and sex differences of white matter and behavioral development through adolescence: A longitudinal diffusion tensor imaging (DTI) study.* NeuroImage, 2014. **92**: p. 356-368.
[5] de Groot, M., et al., *White Matter Degeneration with Aging: Longitudinal Diffusion MR Imaging Analysis.* Radiology, 2015: p. 150103.
[6] Pierpaoli, C., et al., *Water diffusion changes in Wallerian degeneration and their dependence on white matter architecture.* Neuroimage, 2001. **13**(6): p. 1174-1185.
[7] Wheeler-Kingshott, C.A. and M. Cercignani, *About "axial" and "radial" diffusivities.* Magnetic Resonance in Medicine, 2009. **61**(5): p. 1255-1260.
[8] Douaud, G., et al., *DTI measures in crossing-fibre areas: Increased diffusion anisotropy reveals early white matter alteration in MCI and mild Alzheimer's disease.* NeuroImage, 2011. **55**(3): p. 880-890.
[9] Behrens, T., et al., *Probabilistic diffusion tractography with multiple fibre orientations: What can we gain?* Neuroimage, 2007. **34**(1): p. 144-155.
[10] Caan, M.W., et al., *Estimation of diffusion properties in crossing fiber bundles.* Medical Imaging, IEEE Transactions on, 2010. **29**(8): p. 1504-1515.
[11] Assaf, Y. and P.J. Basser, *Composite hindered and restricted model of diffusion (CHARMED) MR imaging of the human brain.* NeuroImage, 2005. **27**(1): p. 48-58.
[12] Hofman, A., et al., *The Rotterdam Study: 2016 objectives and design update.* European journal of epidemiology, 2015. **30**(8): p. 661-708.
[13] Ikram, M.A., et al., *The Rotterdam Scan Study: design and update up to 2012.* Eur J Epidemiol, 2011. **26**(10): p. 811-24.
[14] Jenkinson, M. and S. Smith, *A global optimisation method for robust affine registration of brain images.* Medical image analysis, 2001. **5**(2): p. 143-156.
[15] Leemans, A. and D.K. Jones, *The B-matrix must be rotated when correcting for subject motion in DTI data.* Magnetic Resonance in Medicine, 2009. **61**(6): p. 1336-1349.
[16] Reuter, M. and B. Fischl, *Avoiding asymmetry-induced bias in longitudinal image processing.* Neuroimage, 2011. **57**(1): p. 19-21.
[17] Smith, S.M., et al., *Tract-based spatial statistics: Voxelwise analysis of multi-subject diffusion data.* NeuroImage, 2006. **31**(4): p. 1487-1505.
[18] Jbabdi, S., T.E. Behrens, and S.M. Smith, *Crossing fibres in tract-based spatial statistics.* Neuroimage, 2010. **49**(1): p. 249-256.
[19] Mori, S., et al., *Stereotaxic white matter atlas based on diffusion tensor imaging in an ICBM template.* Neuroimage, 2008. **40**(2): p. 570-82.